I&EC research
Industrial & Engineering Chemistry Research

pubs.acs.org/IECR
Article

Development of a Hybrid Gene Regulatory Network−Bioprocess Model to Enhance the Prediction of Bioethanol Production by *Saccharomyces cerevisiae*

Marianna Christodoulou, Pavlos S. Stephanou, and Michalis Koutinas*

Cite This: https://doi.org/10.1021/acs.iecr.5c01640

ABSTRACT: Albeit bioprocess kinetics are typically predicted using empirical and unstructured models, a gap still exists in connecting bioprocess performance to the molecular events that control the efficiency of bioethanol production using *Saccharomyces cerevisiae*. Herein, a hybrid genetic regulatory network (GRN)−bioprocess model is proposed, predicting transcription from important genes (*HXK2*, *PDC5*, and *ADH1*) involved in the glucose-sensing, glycolysis, and bioethanol production processes, associating glucose consumption as well as biomass and bioethanol production rates to the regulatory events that control bioprocess kinetics. Parameter estimation and validation of the hybrid GRN−bioprocess model were conducted in batch trials supplemented with varying glucose contents via quantification of gene transcription levels. Calculation of the normalized root mean square error (NRMSE) confirmed that the hybrid model developed could accurately predict bioethanol production as opposed to the Monod model. NRMSE values ranged between 0.57−0.91 and 0.60−10.09 for the hybrid and Monod models, respectively, indicating enhanced performance of the novel approach proposed, which improved biomass concentration prediction by 89.4%, glucose concentration prediction by 16.2%, and bioethanol concentration prediction by 60.7% in the experiment conducted using an initial glucose content of 40 g L^{-1}. The hybrid model introduced nonconstant transcription-dependent biomass and product yields as novel functions regulated by the plethora of interactions between the regulatory molecules of the pathways involved, offering substantially improved bioprocess prediction. The proposed framework advances our comprehension of the dynamic properties of bioethanol fermentation via consideration of complex cellular mechanisms controlling the synthesis of rate-limiting enzymes, which are typically ignored by the empirical/unstructured models often applied, providing a systematic understanding of bioethanol manufacture.

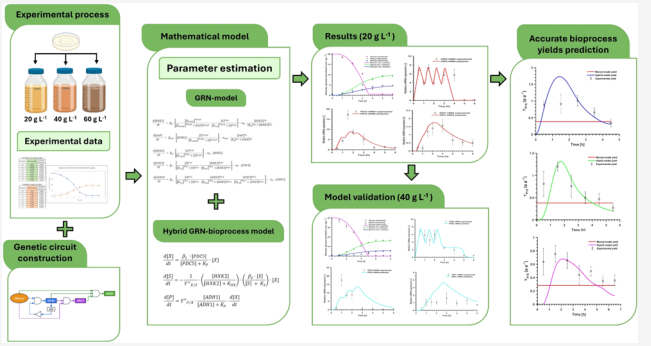

1. INTRODUCTION

Bioethanol stands as a prominent alternative to the use of fossilized hydrocarbons, incorporating renewable nature and eco-friendly features.[1] The rapid development of microbial bioethanol production has demonstrated that *Saccharomyces cerevisiae* constitutes an important candidate for scaling up biofuel production, utilizing glucose as the primary energy source via alcoholic fermentation.[2] The industrial application of the aforementioned yeast could be attributed to properties that include efficiency in a wide range of temperatures (25−39 °C), the capacity to grow under acidic environments with a pH range between 4−6, and tolerance to diverse types of stresses.[3,4]

Previous studies have established that biosynthesis products are usually coupled to microbial growth kinetics and thus account for the fact that the synthesis of specific intracellular molecules in mathematical models could enhance the prediction of the kinetic properties of a microorganism.[5−7] Gene expression is regulated by genetic regulatory networks (GRNs), where genes are transcribed into mRNA and further translated into proteins. The complexity of GRNs involving diverse types of molecules underscores their significance in developing advanced mathematical models that capture diverse biological functions.[8] Moreover, considerable progress has been attained utilizing analytical and computational methods to describe the response of complex GRNs in *S. cerevisiae*, including Bayesian networks, Boolean networks, and ordinary differential equations (ODEs).[9−11] Bayesian models are computationally demanding for complex systems and large data sets,[12−14] while Boolean models oversimplify complex biological processes due to their binary nature (true or false).

Received: April 22, 2025
Revised: July 17, 2025
Accepted: July 21, 2025

Given these limitations, genetic circuits that include ODEs demonstrate enhanced biological realism in comparison with other models, potentially attributed to the intracellular processes considered that account for the inherent complexities of gene expression, protein interactions, and feedback loops.[15,16]

Integrating advanced genetic techniques with mathematical models can advance our comprehension of biological processes, enhancing biological understanding from descriptive to mathematical reasoning.[17] Although a wide range of Monod-based or other unstructured mathematical models have been employed to predict fermentation using the industrial workhorse *S. cerevisiae*,[18,19] in batch fermentation, multiple reactions occur in a short period of time, resulting in a complex biosystem controlling bioprocess performance.[20] Thus, a gap still exists in linking the performance of bioprocesses employing specific strains to the molecular events that regulate the efficiency of bioethanol production.

Monitoring the dynamic response of mRNA expression by important genes for bioethanol fermentation was driven by the fact that mRNA serves as a class of biomolecules, exerting control over the subsequent processes that regulate protein synthesis and enzymatic activity,[21,22] constituting mRNA not only as a valuable marker for assessing gene regulatory events but also as an effective element for predicting bioprocess reaction kinetics.[23] Thus, striving to construct a hybrid model that applies ODEs to simulate molecular events, employing Hill functions as input functions, may provide a more accurate description of the cooperative interactions of DNA elements inside the cell.[8,24,25] The current study established a hybrid model connecting molecular to macroscale events in *S. cerevisiae* during bioethanol fermentation. The construction of a GRN model inclusive of expression from critical pathways, such as the glucose-sensing process, the pathway of glycolysis, and the bioethanol production route, constitutes an innovation aiming at advancing the understanding of intracellular activities pertinent to bioprocess kinetics. The hybrid GRN−bioprocess model proposed was subsequently parametrized and validated by using three distinct batch experiments with different initial glucose concentrations. Furthermore, the prediction of the hybrid model was compared against the Monod model, which has been previously used to simulate bioethanol fermentation processes.[26−28]

2. EXPERIMENTAL SECTION

2.1. Microorganism and Growing Conditions. *S. cerevisiae* strain DSMZ 2155 was obtained from the Leibniz Institute DSMZ-German Collection of Microorganisms and Cell Cultures (Braunschweig, Germany). The yeast was maintained at −80 °C in glycerol stock cultures, and prior to the experiment, it was cultured in a liquid medium consisting of (g L^{-1}): glucose 20, yeast extract 10, and peptone 20. The inoculum was incubated at 30 °C in an orbital shaker stirred at 100 rpm for 18 h. All chemicals used were purchased from Sigma-Aldrich Company Ltd. (Dorset, UK) and were of ANALAR grade.

2.2. Batch Bioethanol Fermentations. Bioethanol fermentations were conducted in batch mode using 250 mL serum bottles. Precultured cells were harvested via centrifugation at 4000 rpm for 15 min, and 1 g of wet biomass was transferred to serum bottles, which were tightly sealed with screw caps and contained 250 mL of fermentation media. Fermentations were conducted using liquid media, which were prepared in 50 mmol L^{-1} citrate buffer at pH 4.8 and consisted of (g L^{-1}): yeast extract 10, peptone 20, and varying glucose concentration (20, 40, and 60 g L^{-1}) depending on the requirements of each experiment. All experiments were performed in triplicate, while two samples were analyzed for each replicate, constituting analyses of 18 samples at each time point. All fermentations were conducted at 30 °C in an orbital shaker and stirred at 100 rpm until glucose depletion.

2.3. Isolation of Total RNA, cDNA Synthesis and Real-Time RT-qPCR (RT-qPCR). RT-qPCR analysis was performed to determine the mRNA expression levels of hexokinase 2 (*HXK2*), pyruvate decarboxylase 5 (*PDC5*), and alcohol dehydrogenase 1 (*ADH1*) genes in the experiments conducted. During the sampling process, duplicate samples of 2 mL were collected at each time point and centrifuged at 9000 rpm for 10 min at 4 °C, and the supernatant solution was removed. Subsequently, the cell pellet was immediately quenched in liquid N_2 for 10 min and stored at −80 °C until further use. Total RNA was isolated from quenched cells, using RNeasy Mini Kit (Qiagen, Germany) according to the manufacturer's instructions and eluted in 40 μL of RNAase-free water.[29] Following the extraction process, total RNA was used for cDNA synthesis, which was conducted using SweScript RT II First Strand cDNA Synthesis Kit (Servicebio, China) and an Oligo (dt) 18 primer (100 μM) applied to obtain the highest yield of full-length cDNA.[30,31]

For RT-qPCR analysis, 1.4 μL of cDNA (40 ng μL^{-1}) was mixed with 10 μL of FastGene ICGreen 2× PCR Universal Mix, 0.8 μL of forward primer (10 μM), 0.8 μL of reverse primer (10 μM), and 7 μL of nuclease-free water. The primer sequences used are displayed in the Supporting Information (Table S1). RT-qPCR reaction was carried out according to the following protocol: predegeneration at 95 °C for 2 min, followed by 40 cycles of degeneration at 95 °C for 5 s and annealing-extension at 60 °C for 30 s. A melting curve was generated for each reaction in order to ensure the specificity of each PCR product. cDNA synthesis and RT-qPCR were performed using a SensoQuest labcycler (SensoQuest GmbH, Göttingen, Germany) and qTower^{3}G real-time PCR (Analytik Jena, Jena, Germany), respectively. *RDN18* was used as the housekeeping gene, and its expression was employed to normalize the cycle threshold (CT) values of all genes tested (eqs 1−3). $C_{T,gene}$ corresponds to the CT values of *HXK2*, *PDC5*, and *ADH1*, respectively, while $C_{T,ref}$ indicates the CT value obtained for *RDN18*. The sample obtained at 0 h was used as the calibrator in eq 2 to normalize the $\Delta C_{T,gene}$ value of each gene at all time points assessed. Subsequently, the normalized level of each gene's mRNA expression (NE_{gene}) was calculated using eq 3.[31]

$$\Delta C_{T,gene} = C_{T,gene} - C_{T,ref} \quad (1)$$

$$\Delta\Delta C_{T,gene} = \Delta C_{T,gene} - \Delta C_{T,gene}(\text{calibrator, time 0 h}) \quad (2)$$

$$NE_{gene} = 2^{-\Delta\Delta CT,gene} \quad (3)$$

2.4. Determination of Biomass, Glucose, and Bioethanol Concentration. Culture samples were collected aseptically and centrifuged at 9000 rpm for 10 min. The resulting supernatant was collected and filtered by using 0.2 μm syringe filters to quantify the glucose and bioethanol contents. The cell pellet was utilized to determine the biomass concentration, using a V-770 UV−visible/NIR spectropho-

https://doi.org/10.1021/acs.iecr.5c01640
Ind. Eng. Chem. Res. XXXX, XXX, XXX−XXX

Table 1. Model Parameters and Estimated Values

symbol	definition	equation	value	symbol	definition	equation	value
β_H	maximal activity of *HXK2* [h^{-1}]	4, 6	22.23	$n_{H,P}$	steepness of the function of *HXK2* and *PDC5* [−]	7	7.27
$n_{S,H}$	steepness of the function of *S* and *HXK2* [−]	4, 6	7.99	$K_{H,P}$	activation coefficient of *PDC5* by *HXK2* [−]	7	4.82
$K_{S,H}$	activation coefficient of *HXK2* by *S* [−]	4, 6	3.98	α_P	mRNA degradation rate of *PDC5* [h^{-1}]	7	0.73
α_H	mRNA degradation rate of *HXK2* [h^{-1}]	4, 6	8.74	β_A	maximal activity of *ADH1* [h^{-1}]	8	2.94
K_H	activation coefficient of *HXK2* [−]	4	0.03	$n_{S,A}$	steepness of the function of *S* and *ADH1* [−]	8	7.94
n_H	steepness of the function of *HXK2* [−]	4	7.98	$K_{S,A}$	activation coefficient of *ADH1* by *S* [−]	8	15.11
β_{G6P}	maximal activity of G6P [h^{-1}]	5	2.11	$n_{H,A}$	steepness of the function of *HXK2* and *ADH1* [−]	8	1.58
$n_{S,G6P}$	steepness of the function of *S* and G6P [−]	5	8	$K_{H,A}$	activation coefficient of *ADH1* by *HXK2* [−]	8	3.75
$K_{S,G6P}$	activation coefficient of G6P by *S* [−]	5	0.1	$n_{P,A}$	steepness of the function of *PDC5* and *ADH1* [−]	8	1.64
$n_{H,G6P}$	steepness of the function of *HXK2* and G6P [−]	5	8.08	$K_{P,A}$	activation coefficient of *ADH1* by *PDC5* [−]	8	0.81
$K_{H,G6P}$	activation coefficient of G6P by *HXK2* [−]	5	0.55	α_A	mRNA degradation rate of *ADH1* [h^{-1}]	8	0.37
α_{G6P}	mRNA degradation rate of G6P [h^{-1}]	5	11.69	β_1	maximum specific growth rate of biomass based on *PDC5* [h^{-1}]	9	1.42
n_G	steepness of the function of G6P [−]	5	8.08	K_P	saturation constant for *PDC5* [−]	9	1.18
K_G	activation coefficient of G6P [−]	5	0.11	$Y''_{X/S}$	transcription-dependent biomass yield [$g_X\ g_S^{-1}$]	9	0.21
$n_{S,H2}$	steepness of the function of *S* and *HXK2* [−]	6	2.5	K_{HX}	saturation constant for *HXK2* [−]	10	1.14
$K_{S,H2}$	activation coefficient of *HXK2* by *S* [−]	6	9.8	β_2	maximum specific growth rate of biomass based on glucose availability [h^{-1}]	10	0.45
β_P	maximal activity of *PDC5* [h^{-1}]	7	18.51	K_2	saturation constant of glucose [$g\ L^{-1}$]	10	0.83
$n_{S,P}$	steepness of the function of *S* and *PDC5* [−]	7	4.99	$Y''_{P/X}$	transcription-dependent product yield [$g_P\ g_X^{-1}$]	11	4.96
$K_{S,P}$	activation coefficient of *PDC5* by *S* [−]	7	14.74	K_A	saturation constant for *ADH1* [−]	11	1.62

tometer (JASCO Corporation, Tokyo, Japan) correlating the optical density (600 nm) obtained and the dry weight of *S. cerevisiae* using a previously established calibration curve.

High-pressure liquid chromatography (HPLC) analysis was employed for the determination of glucose concentration using a Shimadzu Nexera 40 system (Shimadzu, UK) equipped with a Shimadzu RID-20A detector, a Shimadzu SOL-40 C autosampler, and a RHM column oven. The column was eluted isocratically at a rate of 0.5 mL min^{-1} employing an organic analysis column (Rezex RHM-Monosaccharide H+ (8%) column, Phenomenex) with sterilized water at 40 °C and 10 μL of injection volume. Bioethanol production was monitored through gas chromatography (GC) using a Shimadzu GC-2014 (Shimadzu, Milton Keynes, UK) with a flame ionization detector and a 30 m long Zebron ZB-5 capillary column (Phenomenex, Macclesfield, UK) with 0.25 mm internal diameter. The bioethanol content of the samples was extracted into hexane employing vortex agitation to mix 1 mL of filtered sample with 2 mL of solvent, and 1 μL of the extract was injected. The temperature of the column was maintained constant at 40 °C for 2.5 min, followed by an increase of 30 °C min^{-1} up to 160 °C, while it was maintained at 160 °C for an additional 5 min.

3. THEORETICAL BASIS

3.1. Statistical Analysis of mRNA Expression Data. The objective of statistical analysis was to elucidate the relative mRNA expression profile of all genes. One-way ANOVA analysis was conducted using a significance level set at $p < 0.05$.

3.2. GRN−Bioprocess Model Predicting Relative Gene Expression. The initial steps of the model development process involved the establishment of gene expression eqs (eqs 4−8) derived from biological knowledge, using Hill functions[32] as input functions for each gene. Glucose concentration constitutes an important variable, while additional parameters employed for each gene included the maximal activity (β), the degradation rate (α), the Hill coefficient (n) that determines the steepness of each function, and the activation coefficient (K) that is influenced by the relative expression of any other gene involved.[32] Model parameters presented in Table 1 were determined by fitting model predictions against the data obtained from a batch experiment that employed a 20 g L^{-1} initial glucose concentration. The relative mRNA expression of the *HXK2* gene in eq 4 presents the gene's activity affected by glucose-6-phosphate (G6P) to describe an oscillatory response of *HXK2* based on Goodwin's approach.[33] The abundance of the metabolite G6P implemented in the phosphorylation of glucose inhibits *HXK2* through a feedback loop, causing deceleration in the glycolysis process for a specific period of time.[34] Another possible scenario suggests that the accumulation of G6P leads to the accumulation of trehalose-6-phosphate, which inhibits the enzyme activity of HXK2 and decreases the glycolysis rate.[35] Moreover, G6P has been proposed to regulate glucose repression through the pathway of SNF1/Mig1, which is responsible for responding to glucose availability, affecting the utilization of different carbon sources.[36] Based on these findings, *HXK2* can control the glycolysis rate influenced by the oscillatory response of the system.[24,37,38] Nonetheless, when the relative mRNA expression of the gene does not exhibit oscillatory behavior, due to the presence of higher than 20 g L^{-1} glucose concentrations, eq 4 is replaced by eq 6 in the model, where

https://doi.org/10.1021/acs.iecr.5c01640
Ind. Eng. Chem. Res. XXXX, XXX, XXX−XXX

HXK2 activity is stimulated solely by the presence of the substrate. The activity of *PDC5* and *ADH1* is expressed in eqs 7 and 8, respectively.

$$\frac{d[HXK2]}{dt} = \beta_H \cdot \left[\frac{[K_{H,G6P}]^{n_{H,G6P}}}{[K_{H,G6P}]^{n_{H,G6P}} + [G6P]^{n_{H,G6P}}} \cdot \frac{[S]^{n_{S,H}}}{[K_{S,H}]^{n_{Glu,H}} + [S]^{n_{S,H}}} \right] - \alpha_H \cdot \frac{[HXK2]^{n_H}}{[K_H]^{n_H} + [HXK2]^{n_H}} \quad (4)$$

$$\frac{d[G6P]}{dt} = \beta_{G6P} \cdot \left[[HXK2] \cdot \frac{[S]^{n_{S,G6P}}}{[K_{S,G6P}]^{n_{S,G6P}} + [S]^{n_{S,G6P}}} \right] - \alpha_{G6P} \cdot \frac{[G6P]^{n_G}}{[K_G]^{n_G} + [G6P]^{n_G}} \quad (5)$$

$$\frac{d[HXK2]}{dt} = \beta_H \cdot \left[\frac{[S]^{n_{S,H2}}}{[K_{S,H2}]^{n_{S,H2}} + [S]^{n_{S,H2}}} \right] - \alpha_H \cdot [HXK2] \quad (6)$$

$$\frac{d[PDC5]}{dt} = \beta_P \cdot \left[\frac{[S]^{n_{S,P}}}{[K_{S,P}]^{n_{S,P}} + [S]^{n_{S,P}}} \cdot \frac{[HXK2]^{n_{H,P}}}{[K_{H,P}]^{n_{H,P}} + [HXK2]^{n_{H,P}}} \right] - \alpha_P \cdot [PDC5] \quad (7)$$

$$\frac{d[ADH1]}{dt} = \beta_A \cdot \left[\frac{[S]^{n_{S,A}}}{[K_{S,A}]^{n_{S,A}} + [S]^{n_{S,A}}} \cdot \frac{[HXK2]^{n_{H,A}}}{[K_{H,A}]^{n_{H,A}} + [HXK2]^{n_{Ho,A}}} \cdot \frac{[PDC5]^{n_{P,A}}}{[K_{P,A}]^{n_{P,A}} + [PDC5]^{n_{P,A}}} \right] - \alpha_A \cdot [ADH1] \quad (8)$$

3.3. Hybrid GRN−Bioprocess Model. The main objective in the current work was to link macroscale events, such as biomass production (X), glucose consumption (S), and bioethanol production (P), to the transcriptional responses of the GRN model constructed, as shown in eqs 9−11. In the context of eq 9, the expression of *PDC5* was correlated with pyruvate and biomass production. Moreover, *HXK2* transcription serves an important role in initiating the glycolysis pathway, and its inclusion in the hybrid model (eq 10) was necessary, as it regulates glucose consumption. The gene associated with bioethanol production, denoted as *ADH1*, was implemented in eq 11, where it was linked to product (bioethanol) formation.

$$\frac{d[X]}{dt} = \frac{\beta_1 \cdot [PDC5]}{[PDC5] + K_P} \cdot [X] \quad (9)$$

$$\frac{d[S]}{dt} = -\frac{1}{Y''_{X/S}} \cdot \left(\frac{[HXK2]}{[HXK2] + K_{HX}} \right) \cdot \left(\frac{\beta_2 \cdot [S]}{[S] + K_2} \right) \cdot [X] \quad (10)$$

$$\frac{d[P]}{dt} = Y''_{P/X} \cdot \frac{[ADH1]}{[ADH1] + K_A} \cdot \frac{d[X]}{dt} \quad (11)$$

3.4. Monod Model. The Monod model presented in eqs 12−15 could be employed to simulate the concentrations of biomass, glucose, and bioethanol in the bioprocess, respectively.[26,27,39] The specific growth rate (μ) is defined in eq 12, μ_{max} is the maximum specific growth rate, S constitutes substrate concentration, K_S comprises the saturation constant, X is the biomass concentration, $Y_{X/S}$ denotes the biomass yield, P is the product concentration, and $Y_{P/X}$ is the product yield.[28] The main difference between the structure of eqs 9−11 and those of the Monod model (eqs 12−15) lies in the incorporation of the predicted relative mRNA expression of each gene, as derived from eqs 4−8.

$$\mu = \mu_{max} \cdot \frac{[S]}{K_S + [S]} \quad (12)$$

$$\frac{d[X]}{dt} = \mu \cdot [X] \quad (13)$$

$$\frac{d[S]}{dt} = -\frac{1}{Y_{X/S}} \cdot \frac{d[X]}{dt} \quad (14)$$

$$\frac{d[P]}{dt} = Y_{P/X} \cdot \frac{d[X]}{dt} \quad (15)$$

3.5. Parameter Estimation and Assessment of the Hybrid GRN-Bioprocess and Monod Models. The numerical solution of the system of coupled ODEs (eqs 4−15) was obtained using the ode45 solver of MATLAB (version R2022b, Mathworks). The values of model parameters were obtained by fitting model predictions against the experimental data under batch operation using MATLAB linear least-squares curve fit algorithm lsqcurvefit.[40] Initial parameter guesses were set to the mean between the lower and upper bound values for each parameter, with available literature values serving as a basis for optimization. The optimization process refined these parameters to minimize the discrepancy between the model's prediction and the experimental data. The optimized parameters obtained from fitting the model to the experiment conducted using an initial concentration of 20 g L^{-1} were subsequently used without further modifications to provide model predictions in experiments conducted using initial glucose concentrations of 40 and 60 g L^{-1}. The lsqcurvefit solver minimizes the error between the observed data points ($y_{ob,i}$) and the model's prediction for all time points i = 1,···, ni based on the parameter values $f(x_i$,params), as given by eq 16. Once the parameters were set, the sole variable that differed between each model prediction was the initial glucose concentration.

$$\text{lsqcurvefit error} = \sum_{i=1}^{n} [y_{ob,i} - f(x_i, \text{params})]^2 \quad (16)$$

As a metric of quality of the fit to the observed data, the NRMSE (normalized root mean square error) metric was employed to conduct a comparative analysis between Monod and the hybrid GRN−bioprocess models. The NRMSE is related to the lsqcurvefit error, and it is defined in eq 17, where $y_{ob,max}$ and $y_{ob,min}$ compute the maximum and minimum experimental data values, respectively. If the prediction algorithm exhibits a zero NRMSE value, a flawless model is indicated, while a value approaching unity signifies that the model's prediction exhibits errors that are comparable to the variability of the experimental data. On the contrary, when the NRMSE value exceeds unity, the model deviations from the experimental data surpass the range of the values observed, rendering it unfit for practical use.[25,41]

https://doi.org/10.1021/acs.iecr.5c01640
Ind. Eng. Chem. Res. XXXX, XXX, XXX−XXX

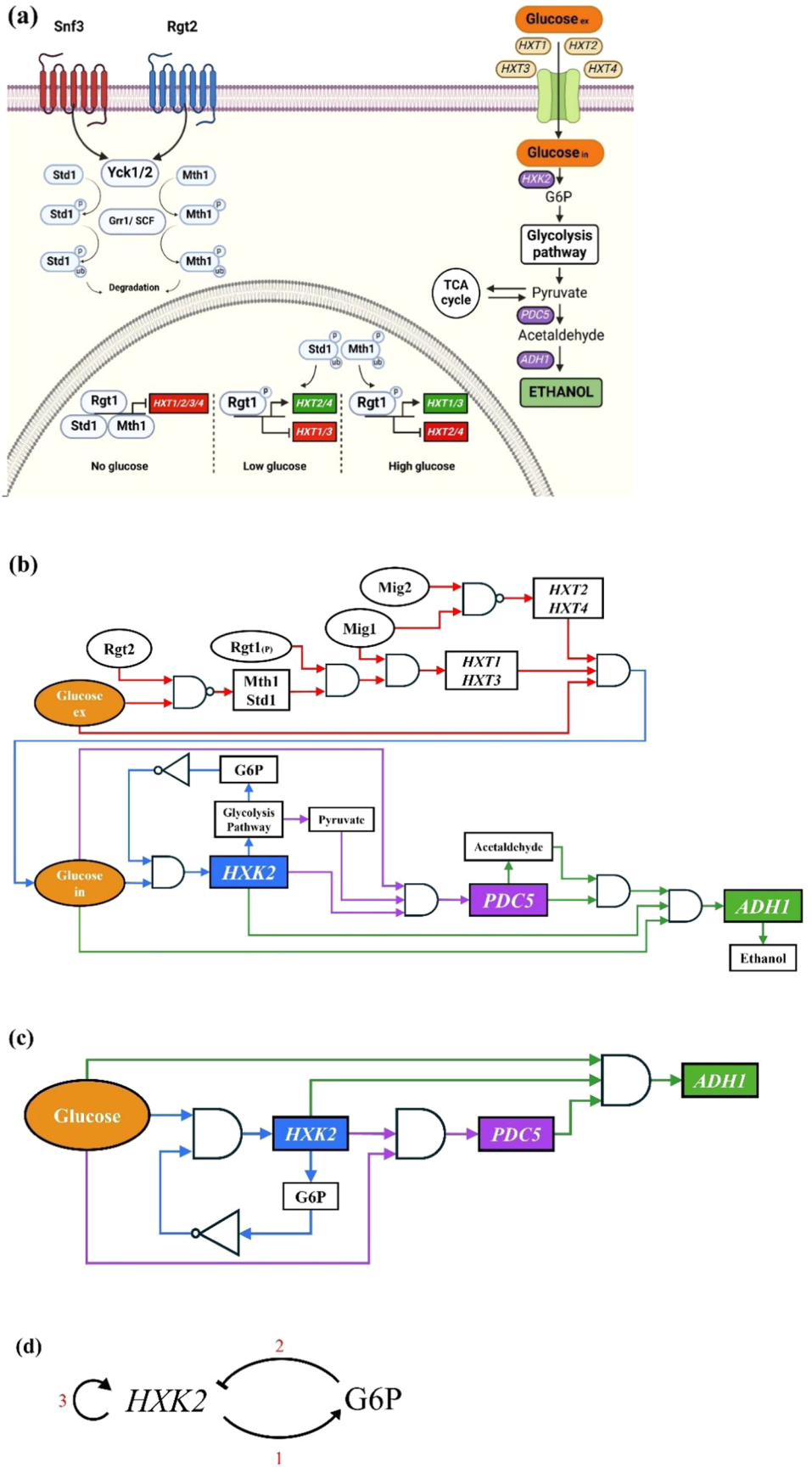

Figure 1. Construction of the GRN model. (a) Schematic overview of the key signal transduction events in two major sugar signaling pathways (Snf3/Rgt2 and Snf1/Mig) in *S. cerevisiae*. Arrows with arrowheads: signaling and induction; arrows with hammerheads: repression; circles with P: phosphorylation; circles with Ub: ubiquitination; and purple circles: important genes of glycolysis pathway and bioethanol production process. (b)

https://doi.org/10.1021/acs.iecr.5c01640
Ind. Eng. Chem. Res. XXXX, XXX, XXX−XXX

Figure 1. continued

Logic representation of the transcriptional regulation in *S. cerevisiae* using logic gates representing the signaling pathways and glucose metabolism as a set of genetic circuits transmitting signals between different molecular components. Arrows with arrowheads: signaling; red arrows: sensing pathway; blue arrows: *HXK2* expression; purple arrows: *PDC5* expression; and green arrows: *ADH1* expression. ⬭: INPUT, ▭: OUTPUT, ⊃: AND, ⊃○: NAND, ▷○: NOT. (c) Reduced logic representation, which includes expression from the genes selected (*HXK2*, *PDC5*, and *ADH1*), omitting the rest of the regulatory events described in part (b). Glucose induces the expression of *HXK2*, which is implemented in an inhibitory loop with G6P repressing *HXK2* synthesis. Following the glycolysis pathway, pyruvate induces transcription from *PDC5*, and subsequently, acetaldehyde assists in the expression of *ADH1*. (d) Hypothesized mechanism, describing the oscillatory behavior of *HXK2*, which is involved in a negative feedback loop by G6P under specific glucose concentrations.

$$\mathrm{NRMSE} = \frac{\sqrt{\frac{1}{n}\sum_{i=1}^{n}[y_{ob,i} - f(x_i, \mathrm{params})]^2}}{y_{ob,\max} - y_{ob,\min}} \tag{17}$$

3.6. Biomass and Product Yield Calculation in the Monod Model. The significance of yield requirements is crucial in industrial fermentation, given that process yields are not as easily amendable as compared to the production rate.[42] Monod related biomass formation to substrate consumption by considering a constant term, known as the biomass yield, defined as the rate of biomass production (d_X) divided by the rate of glucose consumption (d_S) (eq 18). Monod also related biomass production with product formation using the product yield defined as the rate of product formation (d_P) divided by the rate of biomass production (d_X) (eq 19).[43] Numerous models assert that the biomass and product yields remain constant throughout the fermentation process.[28,44] Following the specific approach, the parameter estimation imposed on eqs 18 and 19 provided the values of the constant yields related to biomass and bioethanol production, which were equal to 0.23 $g_X\ g_S^{-1}$ and 2.09 $g_P\ g_X^{-1}$, respectively.

$$Y_{X/S} = \frac{d_X}{d_S} \tag{18}$$

$$Y_{P/X} = \frac{d_P}{d_X} \tag{19}$$

3.7. Biomass and Product Yield of the Hybrid GRN−Bioprocess Model. The present study employed the hybrid GRN−bioprocess model to predict bioprocess yields as variables based on the molecular phenomena controlling each metabolic route. Thus, based on eqs 10 and 11, the new transcription-dependent biomass ($Y'_{X/S}$) and product ($Y'_{P/X}$) yields were expressed based on eqs 20 and 21.

$$\frac{1}{Y'_{X/S}} = \frac{1}{Y''_{X/S}} \cdot \frac{[HXK2]}{[HXK2]\cdot K_{HK}} \tag{20}$$

$$Y'_{P/X} = Y''_{P/X} \cdot \frac{[ADH1]}{[ADH1]\cdot K_A} \tag{21}$$

3.8. Percentage of Improvement for Biomass, Glucose, and Bioethanol Concentrations. The NRMSE value was employed to assess the predictive capability of each model according to the experimental data obtained, by calculating the percentage of improvement for biomass, glucose, and bioethanol concentration profile predictions of the hybrid GRN−bioprocess and Monod models. In eq 22,

$$\text{percentage of improvement} = \frac{\mathrm{NRMSE}_{\mathrm{Monod}} - \mathrm{NRMSE}_{\mathrm{hybrid}}}{\mathrm{NRMSE}_{\mathrm{Monod}}} \times 100 \tag{22}$$

$\mathrm{NRMSE}_{\mathrm{hybrid}}$ constitutes the NRMSE value of the hybrid model regarding biomass, glucose, and bioethanol concentrations in each experiment. Similarly, $\mathrm{NRMSE}_{\mathrm{Monod}}$ was used to express the corresponding NRMSE values derived from the Monod model in each trial.

4. RESULTS AND DISCUSSION

4.1. Construction of the Genetic Circuit Model. During alcoholic fermentation, glucose is utilized via the pathway of glycolysis, which is essential for hexose conversion to bioethanol.[45] Based on glucose availability, three distinct signaling cases have been documented: absence of glucose (0 g L^{-1}), low glucose concentrations ($\leq$20 g L^{-1}), and high glucose concentrations (>20 g L^{-1}).[36,46,47] Glucose concentrations close to 20 g L^{-1} could be classified as either low or high, depending on the specific experimental conditions. The onset of the glycolysis pathway occurs when the two hexose transporter homologues (Snf3 and Rgt2) located at the plasma membrane sense glucose outside the cell (Figure 1a). These transporters are responsible for activating different *HXT*s according to glucose availability.[48,49] When the extracellular environment lacks glucose, *HXT*s are repressed by the Rgt1 transcription factor in association with transcriptional repressors Mth1 and Std1.[50] In the presence of glucose, degradation of Mth1 and Std1 leads to Rgt1 phosphorylation, and the *HXT*s are activated,[51] while the glucose-dependent repressor Mig1 represses expression from alternative carbon source catabolic genes.[52,53] At low glucose concentrations, Snf3 prompts the activation of *HXT1* and *HXT3*, while at high glucose concentrations, Rgt2 triggers transcription from *HXT2* and *HXT4*.[54] Following the sensing pathway of glucose, extracellular glucose is transferred by *HXT*s inside the cell, and it is subsequently phosphorylated predominantly by the enzyme HXK2 to the metabolite G6P.[29] Following the glycolysis pathway, the production of pyruvate, along with other complex pathways, contributes to the activation of the tricarboxylic acid (TCA) cycle.[55] The TCA cycle, in conjunction with the complex pathway of cAMP/PKA, pyruvate, acetyl-CoA, and G6P, participates in biomass synthesis during fermentative growth in *S. cerevisiae*.[36,46]

Based on existing biological knowledge of the yeast's complex molecular pathways[56] and the biochemical description in Figure 1a, a single gene was hypothesized to produce the rate-limiting enzyme controlling the rate of each process (*HXK2* for glycolysis, *PDC5* for biomass production, and *ADH1* for bioethanol production). Thus, the GRN illustrated in Figure 1b has been structured as a genetic circuit, which includes logic gates that transmit signals between the different molecules regulating transcription from the relevant rate-limiting gene controlling each pathway. These signals may invert the input (NOT), continue to the output only if two of

https://doi.org/10.1021/acs.iecr.5c01640
Ind. Eng. Chem. Res. XXXX, XXX, XXX−XXX

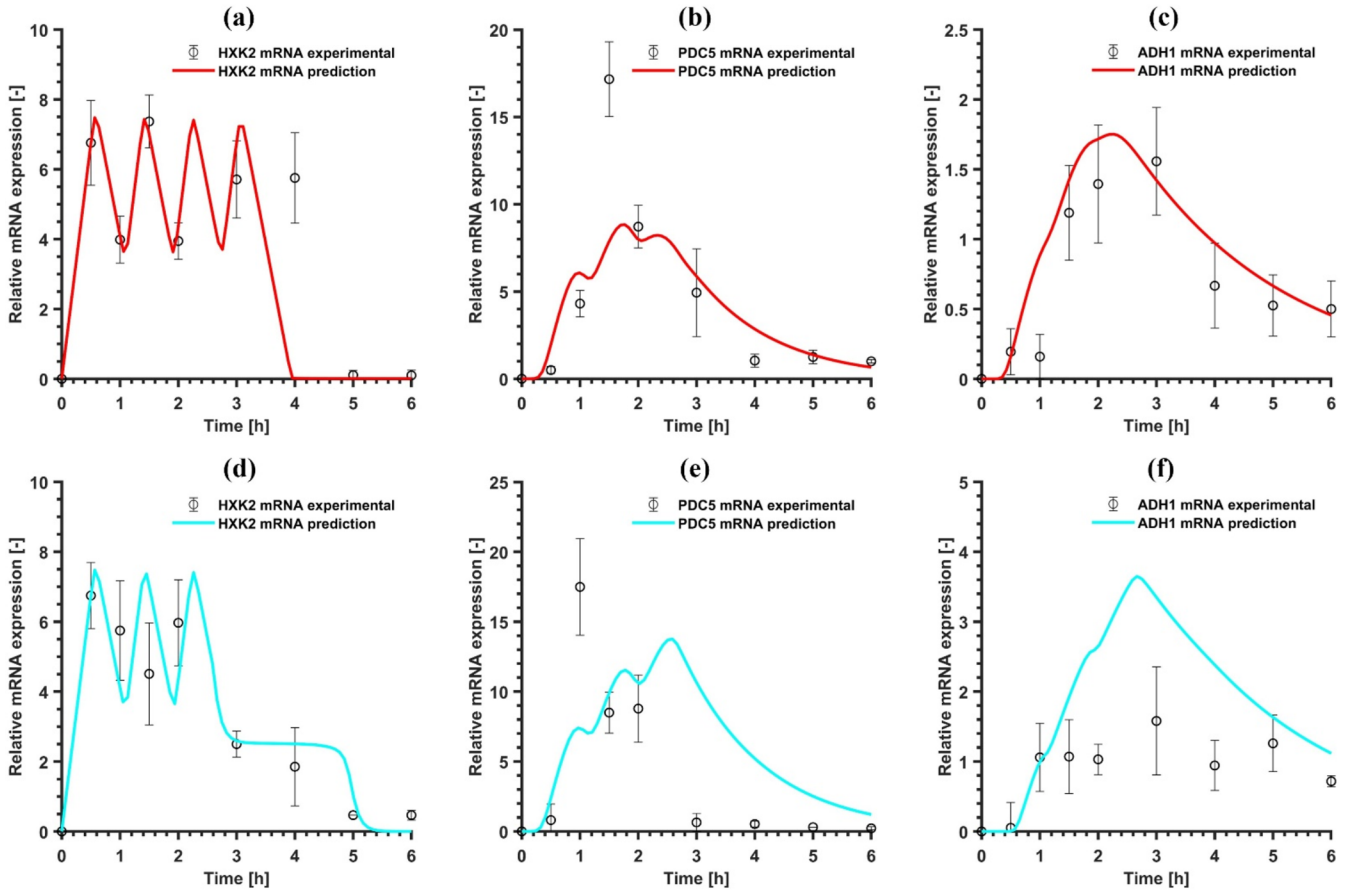

Figure 2. GRN model simulation of transcription from key genes in the bioprocess. Simulations and experimental data of (a) *HXK2*, (b) *PDC5*, and (c) *ADH1* transcription using 20 g L^{-1} of glucose as well as (d) *HXK2*, (e) *PDC5*, and (f) *ADH1* transcription using 40 g L^{-1} of glucose. The results were obtained as an average of six individual measurements at each time point, and the error bars were calculated for standard deviation. Experiments were performed at 30 °C and 100 rpm until glucose depletion.

the inputs are present in high concentration (AND), and invert the output if two of the inputs are present (NAND).[57] Glucose is used as an input that affects the glucose-sensing process, the activation of the *HXT*s, and the glycolysis pathway until bioethanol production. Although regulation in each pathway is more complex compared to the control of transcription from a single gene considered in Figure 1c, the objective here was to simplify the biological behavior by limiting the number of molecules included within the circuit, selectively incorporating those deemed as the most important for each pathway. Thus, expression from a single rate-limiting gene was hypothesized and accounted for in each route. The simplified circuit (Figure 1c) included transcription from *HXK2*, *PDC5*, and *ADH1*, while glucose constituted the input stimulating the whole process.

The expression of the *HXK2* selected is responsible for the onset of glycolysis, and it can be influenced by glucose availability,[58,59] while an oscillatory transcriptional response is expected only at low glucose concentrations as a result of cells continuously adjusting their metabolic state to conserve energy.[37] Although glucose activates *HXK2*, the gene additionally participates in a negative feedback loop under a variety of conditions.[60,61] One possible scenario suggests that the abundance of the metabolite G6P inhibits *HXK2* through a feedback loop, thereby causing deceleration of the glycolysis pathway (Figure 1d).[62] By taking into account the diverse range of factors that impact biomass production, transcription from the specific gene was considered in the model, given that biomass is produced following activation of the glycolytic process and the TCA cycle. Moreover, the *PDC5* gene was selected, given that it is expressed right after pyruvate production and holds a crucial role in the production of bioethanol, while it is additionally related to biomass growth.[63,64] The terminal gene integrated into the circuit comprised *ADH1*, which encodes for the reduction of acetaldehyde to bioethanol during the last step of bioethanol production, and its expression is dependent on glucose utilization.[65−67]

The simulations presented in Figure 2 demonstrated that the relative expression of mRNA produced during glucose metabolism and the targeted genes related to bioethanol production could be adequately predicted. The compared NRMSE values for the relative expression of genes *HXK2*, *PDC5*, and *ADH1* in the GRN model are presented as Supporting Information (Figure S 1d), confirming that the model accurately captured the experimental gene expression data, including NRMSE values lower than 1. ANOVA confirmed statistically significant differences in the mean values of the data at the 95% confidence level ($p < 0.05$, ANOVA analysis has been included as Supporting Information in Table S2), confirming that the *HXK2* gene exhibited oscillatory behavior. Thus, at 20 g L^{-1} initial glucose concentration, three distinct time groups (0.5 + 1.5 h, 1 + 2 h, 3 + 4 h) that included similar mean values were monitored,

https://doi.org/10.1021/acs.iecr.5c01640
Ind. Eng. Chem. Res. XXXX, XXX, XXX−XXX

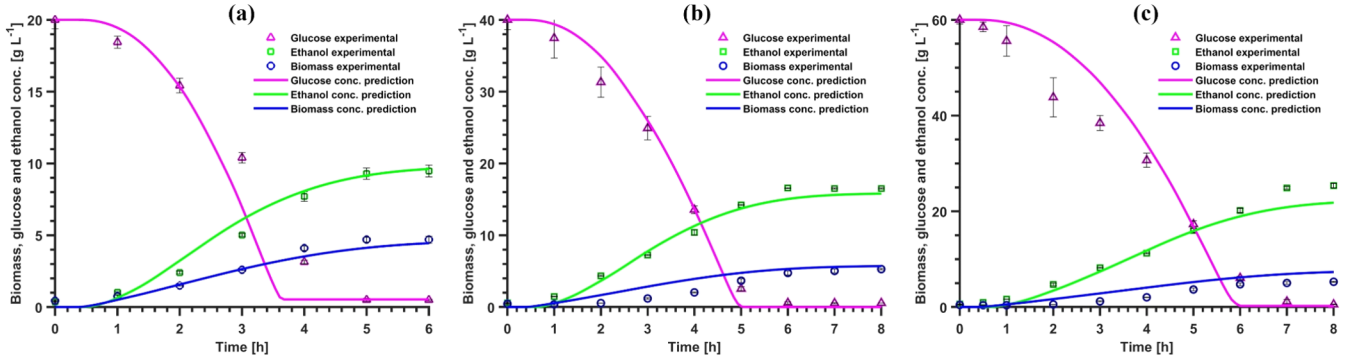

Figure 3. Experimental data and hybrid model's simulation of the bioprocess using *S. cerevisiae* during batch fermentation applying (a) 20 g L^{-1}, (b) 40 g L^{-1}, and (c) 60 g L^{-1} initial glucose concentration. The results were obtained as an average from six individual measurements at each time point, and the error bars were calculated for standard deviation. Experiments were performed at 30 °C and 100 rpm until glucose depletion.

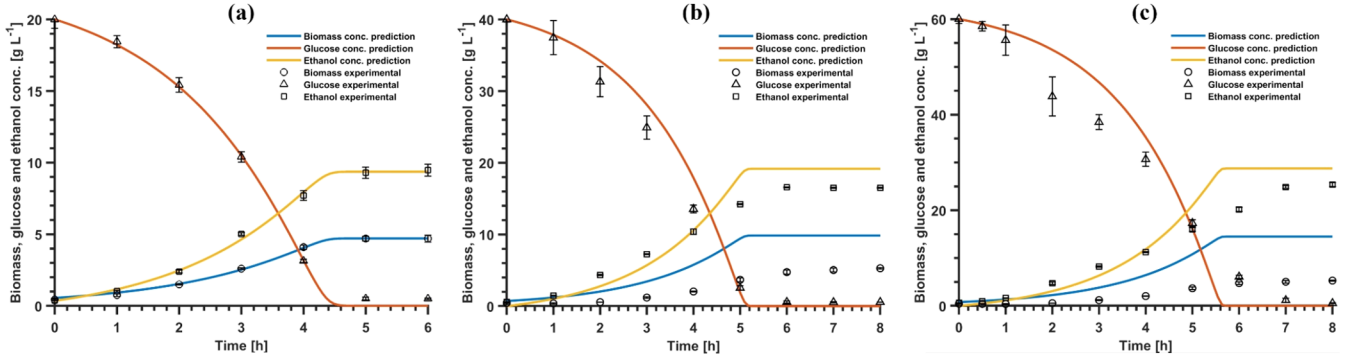

Figure 4. Experimental data and Monod model simulation of the bioprocess using *S. cerevisiae* during batch fermentation applying (a) 20 g L^{-1}, (b) 40 g L^{-1}, and (c) 60 g L^{-1} initial glucose concentration. The results were obtained as an average from six individual measurements at each time point, and the error bars were calculated for standard deviation. Experiments were performed at 30 °C and 100 rpm until glucose depletion.

demonstrating significant differences between each group ($p < 0.05$). Subsequently, a small decrease in the *HXK2* activity shown in Figures 2a,d can lead to decreased utilization of glucose by the glycolytic pathway, impacting the expression of other genes for a specific period of time.[61] Based on *PDC5* relative mRNA concentration prediction presented in Figure 2b for 20 g L^{-1} and Figure 2e for 40 g L^{-1} of initial glucose concentration, the model was capable of predicting the gene's expression, but underpredicted the maximum expression level monitored. Moreover, the activity of *ADH1* is presented in Figure 2c,f for 20 and 40 g L^{-1} of initial glucose concentration, respectively. Prediction of relative mRNA expression from *ADH1* closely predicted the experiment conducted using a 20 g L^{-1} initial glucose concentration. However, although the model could adequately predict the data obtained employing 40 g L^{-1} glucose, the relative mRNA expression was overpredicted between 2 and 4 h of fermentation. Thus, although the overall trend of the model's prediction is accurate, the slight discrepancies monitored could potentially arise due to unknown molecular mechanisms influencing *PDC5* and *ADH1* transcription, which have not yet been described in detail.

4.2. Hybrid GRN−Bioprocess Model Predicting Macroscale Events. The results of the developed hybrid model regarding the macroscale bioprocess performance are illustrated in Figure 3. The parameter values were determined by fitting the model in the experimental data obtained using an initial glucose concentration of 20 g L^{-1} (Figure 3a). The culture exhibited a lag phase of approximately 30 min, which was followed by complete substrate consumption and bioethanol production of 9.3 g L^{-1}. Although the mathematical model closely predicted bioethanol and biomass formation, the concentration of glucose was slightly underpredicted between 3 and 4 h of fermentation. Subsequently, to validate the efficacy of the developed model, the fully parametrized hybrid model was employed to predict the bioprocess using the data of the experiment conducted using 40 g L^{-1} as the initial glucose concentration, confirming the predictive capability of the hybrid approach (Figure 3b). Moreover, regarding the experiment performed using an initial glucose concentration of 60 g L^{-1}, although glucose concentration was overpredicted between 1 and 3 h of fermentation, a close agreement was observed between the model's prediction and the experimental data obtained (Figure 3c). Overall, the proposed hybrid GRN−bioprocess model demonstrated high fidelity in the prediction of all batch trials performed, exhibiting an accurate description of the biosystem under different experimental conditions. The capacity of the hybrid model to accurately capture the dynamics of the bioprocess and the underlying molecular events demonstrated the robustness of the proposed approach.

4.3. Monod Model Simulation and Comparison with the Hybrid GRN−Bioprocess Model. Obtaining the Monod model parameter values required the same fitting methodology as that used for the new hybrid model. Thus, model parameter values were determined by fitting the experimental data obtained using an initial glucose concentration of 20 g L^{-1}, and the parametrized model was applied to predict the experiments

https://doi.org/10.1021/acs.iecr.5c01640
Ind. Eng. Chem. Res. XXXX, XXX, XXX−XXX

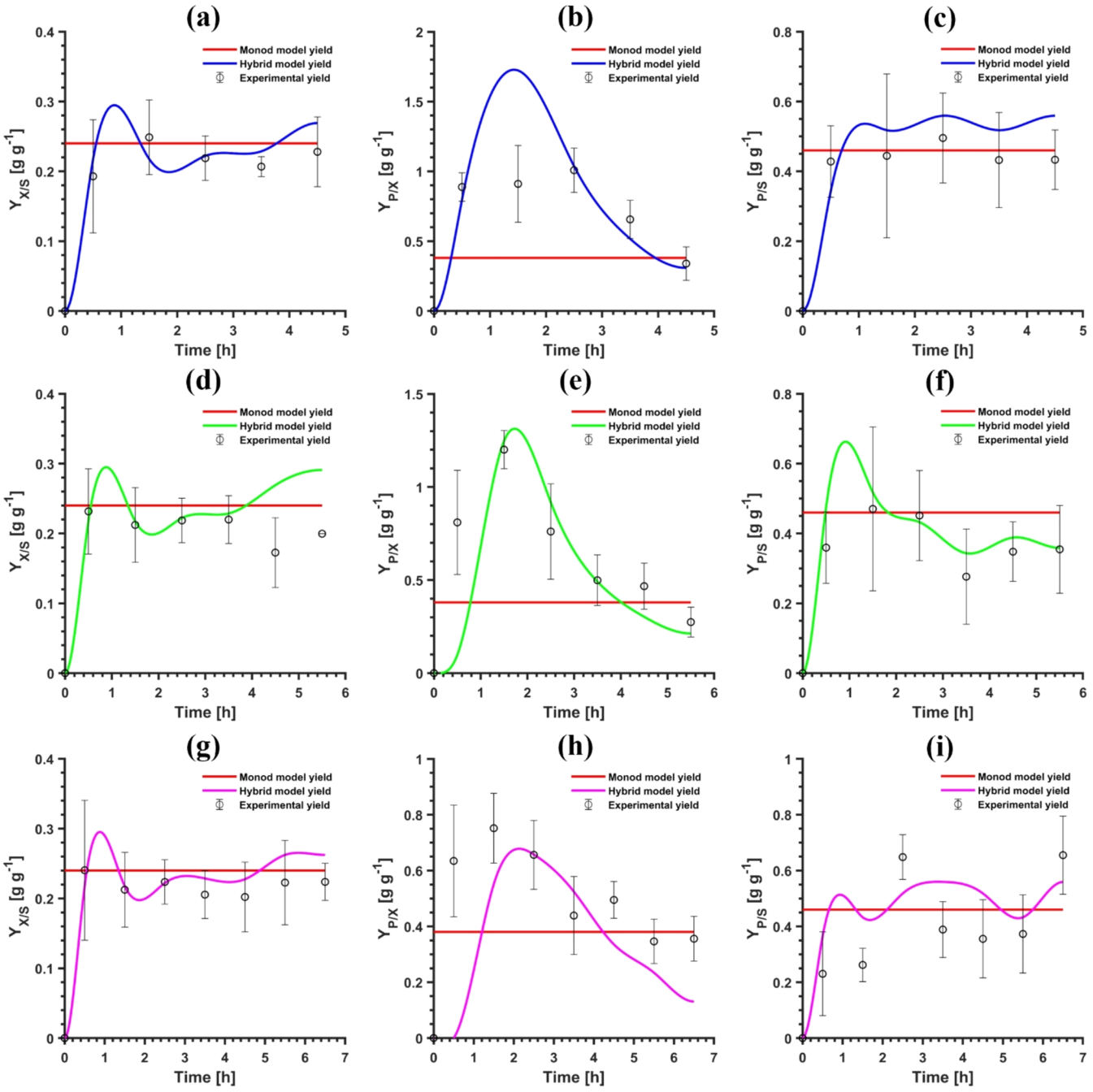

Figure 5. Simulations of biomass and product yields using Monod and hybrid GRN−bioprocess models. 20 g L^{-1} of glucose: (a) $Y_{X/S}$, (b) $Y_{P/X}$, and (c) $Y_{P/S}$; 40 g L^{-1} of glucose: (d) $Y_{X/S}$, (e) $Y_{P/X}$, and (f) $Y_{P/S}$; 60 g L^{-1} of glucose: (g) $Y_{X/S}$, (h) $Y_{P/X}$, and (i) $Y_{P/S}$. The red line in each graph indicates the constant biomass and product yield based on the Monod model. The rest of the colors applied correspond to simulations conducted aiming to predict biomass and product yields utilizing the hybrid model.

conducted employing 40 and 60 g L^{-1} initial glucose concentration. As shown in Figure 4a, the Monod model accurately predicted the experimental data obtained using an initial glucose concentration of 20 g L^{-1} via application of the following parameter values: μ = 0.53 h^{-1}, Ks = 0.63 g L^{-1}, $Y_{X/S}$ = 0.23 g_X g_S^{-1}, and $Y_{P/X}$ = 2.09 g_P g_X^{-1}. All parameter values were in agreement with the typical values reported in the literature in similar Monod models.[27,68] However, as illustrated in Figure 4b,c, for the experiments conducted employing 40 and 60 g L^{-1} of initial glucose concentration, the model closely predicted glucose concentration, while it showed limited accuracy in predicting biomass and bioethanol concentrations.

Literature suggests a diverse array of statistical metrics to evaluate the predictability and performance of mathematical models based on experimental data, as well as for comparing models to determine which best predicts the observed data.[19,41,69,70] Given the nonlinear nature of the proposed model, which includes molecular activities, the NRMSE metric was selected to evaluate the quality and predictive capability of the hybrid GRN−bioprocess and Monod models employed, considering that the specific metric presents the relative value of the absolute error.[71] The compared NRMSE values for the biomass, glucose, and bioethanol concentrations of the hybrid GRN−bioprocess and Monod models are presented in the

https://doi.org/10.1021/acs.iecr.5c01640
Ind. Eng. Chem. Res. XXXX, XXX, XXX−XXX

Supporting Information (Figure S1). In the experiment conducted using an initial glucose concentration of 20 g L^{-1}, the Monod model demonstrated satisfactory NRMSE values for biomass, glucose, and bioethanol concentrations, which accounted for 0.64, 0.66, and 0.61, respectively. However, in the experiment performed using an initial glucose concentration of 40 g L^{-1}, although the NRMSE value of glucose concentration was 0.68, the biomass and bioethanol concentration profiles provided NRMSE values that exceeded the acceptable threshold value (7.08 and 1.73, respectively), which is indicative of the Monod model failing to predict the experimental data, as shown in Figure 4b. A similar response applied to the NRMSE values obtained using the predictions in the experiment conducted employing an initial glucose concentration of 60 g L^{-1}, where the NRMSE values for biomass and bioethanol concentration prediction comprised 10.09 and 1.89, respectively. However, the new hybrid model included satisfactory NRMSE values (less than unity) for the relative mRNA expression profiles predicted for each gene considered in the GRN model (Supporting Information, Figure S1). In the third experiment conducted using an initial glucose concentration of 60 g L^{-1}, it could be noted that the use of the hybrid model yielded an accurate fit with NRMSE values similar to those reported in the rest of the experiments presented.

4.4. Prediction of Biomass and Product Yields Using the Hybrid GRN−Bioprocess Model. Since the consideration of constant biomass and product yields in the Monod model resulted in inconsistencies of model prediction against the experimental data, different studies have demonstrated that incorporating nonconstant yields can significantly improve the accuracy of model prediction. Similarly to the current work, Koutinas et al.[23] developed a hybrid GRN−bioprocess model that substantially improved the prediction of *m*-xylene biodegradation by *Pseudomonas putida* as opposed to the Monod model, which overestimated biomass formation by 32%. The advanced performance of the hybrid approach was achieved via application of nonconstant yields, which were regulated by the synthesis of rate-limiting enzymes hypothesized in each of the pathways considered in the GRN model. Moreover, Tsafrakidou et al.[72] proposed a refined Monod-Logistic model incorporating a nonconstant product yield, which adjusted $Y_{P/X}$ as a function of the maximum substrate concentration applied, effectively capturing the inhibition of bioethanol production monitored at elevated substrate levels. Thus, by calculating the hourly yield based on the experimental data obtained, the prediction of biomass and product yields using the hybrid GRN−bioprocess model was compared against the yields considered in the Monod model (Figure 5).

The simulations compared against the experimental data demonstrated an overall time-dependent behavior. Aiming to validate the predictive capability of the two models applied, NRMSE calculations were conducted. As illustrated in Figure S2 (Supporting Information), the NRMSE values for biomass ($Y_{X/S}$) and product yields ($Y_{P/S}$) were acceptable, exhibiting values below unity. Although $Y_{X/S}$ and $Y_{P/S}$ could be efficiently predicted by both the hybrid GRN−bioprocess and Monod models, $Y_{P/X}$ could be accurately described only by the transcription-dependent yield expression employed in the hybrid model. However, the hybrid GRN−bioprocess model consistently outperformed the Monod model across all three experiments (20, 40, and 60 g L^{-1}) conducted, achieving biomass yield ($Y'_{X/S}$) NRMSE values of 0.10, 0.21, and 0.10, respectively. Nevertheless, the NRMSE values computed for the Monod model ranged between 0.36 and 0.41. A similar pattern was observed for the product yield $Y_{P/S}$, where the hybrid GRN−bioprocess model exhibited NRMSE values between 0.11 and 0.19, while the Monod model's values ranged between 0.34 and 0.42. On the contrary, regarding the product yield ($Y_{P/X}$), although the hybrid GRN−bioprocess model demonstrated moderate predictive capability, incorporating NRMSE values of 0.33, 0.23, and 0.34 for the three experiments conducted, the Monod model exhibited significantly higher and less reliable NRMSE values (1.37−2.12).

The aforementioned results underscore the importance of incorporating the transcription-dependent yields proposed in this work to improve bioprocess prediction. The presence of nonconstant yields can be considered to reduce the errors often generated when constant yields are assumed.[23] Thus, the proposed hybrid GRN−bioprocess model has demonstrated that although yield values can vary under different time periods and conditions, the prediction of important regulatory events could enable an accurate prediction of bioprocess yields during bioethanol manufacture.

4.5. Comparing the Prediction of the Hybrid GRN−Bioprocess and Monod Models. The percentage of improvement of the hybrid GRN−bioprocess model against the Monod model did not exhibit improvement in predicting the experiment conducted using 20 g L^{-1} glucose, given that the predictions of both models were consistent with experimental data. However, significant improvement was noted in the experiment conducted using 40 g L^{-1} glucose, where the hybrid GRN−bioprocess model enhanced by 89.4, 16.2, and 60.7% biomass, glucose, and bioethanol concentration predictions, respectively. Similar improvements were confirmed in the experiment performed using 60 g L^{-1} glucose, where the hybrid GRN−bioprocess model improved by 93.4, 4.7, and 51.9% biomass, glucose, and bioethanol concentration predictions, respectively.

5. CONCLUSIONS

The notable accuracy of the modeling framework proposed in predicting biosystem performance confirmed the significance of employing descriptions of complex regulatory programs for the realization of bioprocesses and their optimal design. The hybrid GRN−bioprocess model enhanced the predictive accuracy of bioethanol manufacture via a simplified description of the molecular events entailed, avoiding detailed representation of the system's complex biological nature. ANOVA analysis confirmed that the *HXK2* gene exhibited oscillatory behavior, while at an initial glucose concentration of 40 g L^{-1}, the model achieved improvements of 89.4, 16.2, and 60.7% in the prediction of biomass, glucose, and bioethanol concentrations as opposed to the Monod model, respectively. The construction of programmable biocatalysts for efficient bioethanol manufacture will necessitate optimizing pertinent GRNs and employing current knowledge of the causality and connectivity of important circuit components that regulate the production rate of value-added commodities to improve mathematical model accuracy. Moreover, capturing nonconstant yields has been enabled, mitigating the errors encountered when constant yields are assumed in unstructured and empirical models, which could limit their relevance to only a specific set of conditions. The hybrid GRN−bioprocess model enables systemic understanding of the biosystem and, in future research, will aim to employ the current modeling

https://doi.org/10.1021/acs.iecr.5c01640
Ind. Eng. Chem. Res. XXXX, XXX, XXX−XXX

framework with significant advances in molecular biology to further improve the design of optimal bioethanol manufacture processes.

■ ASSOCIATED CONTENT

Supporting Information

The Supporting Information is available free of charge at https://pubs.acs.org/doi/10.1021/acs.iecr.5c01640.

A table listing the oligonucleotide primers used in real-time RT-qPCR; a table of ANOVA results indicating oscillatory behavior of the *HXK2* gene; and NRMSE values of the hybrid GRN−bioprocess and Monod models in *S. cerevisiae* fermentations (PDF)

■ AUTHOR INFORMATION

Corresponding Author

Michalis Koutinas − *Department of Chemical Engineering, Cyprus University of Technology, Limassol 3036, Cyprus;* orcid.org/0000-0002-5371-4280; Email: michail.koutinas@cut.ac.cy

Authors

Marianna Christodoulou − *Department of Chemical Engineering, Cyprus University of Technology, Limassol 3036, Cyprus;* orcid.org/0000-0002-2746-3000

Pavlos S. Stephanou − *Department of Chemical Engineering, Cyprus University of Technology, Limassol 3036, Cyprus;* orcid.org/0000-0003-3182-0581

Complete contact information is available at: https://pubs.acs.org/10.1021/acs.iecr.5c01640

Notes

The authors declare no competing financial interest.

■ ACKNOWLEDGMENTS

This research did not receive any specific grant from funding agencies in the public, commercial, or not-for-profit sectors.

■ REFERENCES

(1) Khumsupan, D.; Lin, S.; Huang, Y.; Chen, C.; Chi, H.; Jantama, K.; Lin, H.; Cheng, K. Industrial Crops & Products Creating a Robust and Reusable Cell Immobilization System for Bioethanol Production by Thermotolerant Yeast Using 3D Printing and Soybean Waste. *Ind. Crop. Prod.* **2025**, *224*, No. 120434.

(2) Rastogi, M.; Shrivastava, S. Recent Advances in Second Generation Bioethanol Production: An Insight to Pretreatment, Saccharification and Fermentation Processes. *Renew.Sustain. Energy Rev.* **2017**, *80*, 330−340.

(3) Tanahashi, R.; Nishimura, A.; Kan, K.; Ishizaki, N.; Fujishima, S.; Endo, H.; Takagi, H. Enhancing Freezing Stress Tolerance through Regulation of the Ubiquitin−Proteasome System in *Saccharomyces cerevisiae*. *Fermentation* **2024**, *10*, No. 318.

(4) Zhang, H.; Zhang, P.; Wu, T.; Ruan, H. Bioethanol Production Based on *Saccharomyces cerevisiae*: Opportunities and Challenges. *Fermentation* **2023**, *9*, No. 709.

(5) Buldum, G.; Tsipa, A.; Mantalaris, A. Linking Engineered Gene Circuit Kinetic Modeling to Cellulose Biosynthesis Prediction in *Escherichia coli*: Toward Bioprocessing of Microbial Cell Factories. *Ind. Eng. Chem. Res.* **2020**, *59*, 4659−4669.

(6) Almquist, J.; Cvijovic, M.; Hatzimanikatis, V.; Nielsen, J.; Jirstrand, M. Kinetic Models in Industrial Biotechnology - Improving Cell Factory Performance. *Metab. Eng.* **2014**, *24*, 38−60.

(7) Hatzimanikatis, V.; Emmerling, M.; Sauer, U.; Bailey, J. E. Application of Mathematical Tools for Metabolic Design of Microbial Ethanol Production. *Biotechnol. Bioeng.* **1998**, *58*, 154−161.

(8) Tsipa, A.; Koutinas, M.; Usaku, C.; Mantalaris, A. Optimal Bioprocess Design through a Gene Regulatory Network − Growth Kinetic Hybrid Model: Towards Replacing Monod Kinetics. *Metab. Eng.* **2018**, *48*, 129−137.

(9) Christensen, T. S.; Oliveira, A. P.; Nielsen, J. Reconstruction and Logical Modeling of Glucose Repression Signaling Pathways in *Saccharomyces cerevisiae*. *BMC Syst. Biol.* **2009**, *3*, No. 7.

(10) Kotiang, S.; Eslami, A. Boolean Factor Graph Model for Biological Systems : The Yeast Cell - Cycle Network. *BMC Bioinf.* **2021**, *22*, No. 442.

(11) Haliki, E.; Alpagut Keskin, N.; Masalci, O. Boolean Gene Regulatory Network Model of Centromere Function in *Saccharomyces cerevisiae*. *J. Biol. Phys.* **2019**, *45*, 235−251.

(12) Weglarz-Tomczak, E.; Tomczak, J. M.; Eiben, A. E.; Brul, S. Population-Based Parameter Identification for Dynamical Models of Biological Networks with an Application to *Saccharomyces cerevisiae*. *Processes* **2021**, *9*, No. 98.

(13) Simak, M.; Yeang, C. H.; Lu, H. H. S. Exploring Candidate Biological Functions by Boolean Function Networks for *Saccharomyces cerevisiae*. *PLoS One* **2017**, *12* (10), No. e0185475.

(14) Raue, A.; Kreutz, C.; Theis, F. J.; Timmer, J. Joining Forces of Bayesian and Frequentist Methodology: Joining Forces of Bayesian and Frequentist methodology: A Study for Inference in the Presence of Non-Identifiability. *Philos. Trans. R. Soc. A* **2013**, *371*, No. 20110544.

(15) Saravanan, S.; Syed Ali, M.; Rajchakit, G.; Hammachukiattikul, B.; Priya, B.; Thakur, G. K. Finite-Time Stability Analysis of Switched Genetic Regulatory Networks with Time-Varying Delays via Wirtinger's Integral Inequality. *Complexity* **2021**, *2021*, No. 9540548.

(16) Zhang, L.; Zhang, X.; Xue, Y.; Zhang, X. New Method to Global Exponential Stability Analysis for Switched Genetic Regulatory Networks with Mixed Delays. *IEEE Trans. Nanobioscience* **2020**, *19*, 308−314.

(17) Bailey, J. E. Mathematical Modeling and Analysis in Biochemical Engineering: Past Accomplishments and Future Opportunities. *Biotechnol. Prog.* **1998**, *14* (1), 8−20.

(18) Salakkam, A.; Phukoetphim, N.; Laopaiboon, P.; Laopaiboon, L. Mathematical Modeling of Bioethanol Production from Sweet Sorghum Juice under High Gravity Fermentation: Applicability of Monod-Based, Logistic, Modified Gompertz and Weibull Models. *Electron. J. Biotechnol.* **2023**, *64*, 18−26.

(19) Ünsal, S. B. E.; Tufan, H. N. G.; Canatar, M.; Yatmaz, E.; Yavuz, I.; Germec, M.; Turhan, I. An Evaluation of Mathematical Modeling of Ethanol Fermentation with Immobilized *Saccharomyces cerevisiae* in the Presence of Different Inhibitors. *Processes* **2025**, *13* (3), No. 656.

(20) Salazar, Y.; Valle, P. A.; Rodriguez, E.; Soto-Cruz, N. O.; Paez-Lerma, J. B.; Reyes-Sanchez, F. J. Mechanistic Modelling of Biomass Growth, Glucose Consumption and Ethanol Production by *Kluyveromyces marxianus* in Batch Fermentation. *Entropy* **2023**, *25* (3), 1−36.

(21) Singh, K. P.; Miaskowski, C.; Dhruva, A. A.; Flowers, E.; Kober, K. M. Mechanisms and Measurement of Changes in Gene Expression. *Biol. Res. Nurs.* **2018**, *20* (4), 369−382.

(22) Clarke-Whittet, M.; Rocco, A.; Gerber, A. P. Parameterising Translational Feedback Models of Autoregulatory RNA-Binding Proteins in *Saccharomyces cerevisiae*. *Microorganisms* **2022**, *10* (2), No. 340.

(23) Koutinas, M.; Kiparissides, A.; Silva-Rocha, R.; Lam, M. C.; Martins dos Santos, V. A. P.; de Lorenzo, V.; Pistikopoulos, E. N.; Mantalaris, A. Linking Genes to Microbial Growth Kinetics-An Integrated Biochemical Systems Engineering Approach. *Metab. Eng.* **2011**, *13* (4), 401−413.

(24) Takhaveev, V.; Ozsezen, S.; Smith, E. N.; Zylstra, A.; Chaillet, M. L.; Chen, H.; Papagiannakis, A.; Milias-Argeitis, A.; Heinemann, M. Temporal Segregation of Biosynthetic Processes Is Responsible for

Metabolic Oscillations during the Budding Yeast Cell Cycle. *Nat. Metab.* **2023**, *5* (2), 294−313.
(25) Tsipa, A.; Pitt, J. A.; Banga, J. R.; Mantalaris, A. A Dual-Parameter Identification Approach for Data-Based Predictive Modeling of Hybrid Gene Regulatory Network-Growth Kinetics in *Pseudomonas putida* Mt-2. *Bioprocess Biosyst. Eng.* **2020**, *43* (9), 1671−1688.
(26) Xu, P. Analytical Solution for a Hybrid Logistic-Monod Cell Growth Model in Batch and Continuous Stirred Tank Reactor Culture. *Biotechnol. Bioeng.* **2020**, *117* (3), 873−878.
(27) Khalseh, R. Evaluation of Different Kinetics for Bioethanol Production with Emphasis to Analytical Solution of Substrate Equation. *Theor. Found. Chem. Eng.* **2016**, *50* (4), 392−397.
(28) Zentou, H.; Abidin, Z. Z.; Abdullah Issa, M.; Yunus, R.; Radiah Awang Biak, D. Developing an Integrated Mathematical Model of Fermentation-Pervaporation System for Bioethanol Production. *Chem. Eng. J.* **2023**, *473* (10), No. 145229.
(29) Lesko, M. A.; Chandrashekarappa, D. G.; Jordahl, E. M.; Oppenheimer, K. G.; Bowman, R. W.; Shang, C.; Durrant, J. D.; Schmidt, M. C.; O'Donnell, A. F. Changing Course: Glucose Starvation Drives Nuclear Accumulation of Hexokinase 2 in *S. cerevisiae*. *PLoS Genet.* **2023**, *19* (5), No. e1010745, DOI: 10.1371/journal.pgen.1010745.
(30) Okabayashi, K.; Ogawa, H.; Hirai, Y.; Nagata, K.; Sato, Y.; Narita, T.; Satoh, K.; Makimura, K. Changes in the mRNA Expression of Glycolysis-Related Enzymes of *Candida albicans* during Inhibition of Intramitochondrial Catabolism under Anaerobic Condition. *PLoS One* **2023**, *18* (4), 1−11.
(31) Kyriakou, M.; Christodoulou, M.; Ioannou, A.; Fotopoulos, V.; Koutinas, M. Improvement of Stress Multi-Tolerance and Bioethanol Production by *Saccharomyces cerevisiae* Immobilised on Biochar : Monitoring Transcription from Defence-Related Genes. *Biochem. Eng. J.* **2023**, *195*, No. 108914.
(32) Chen, J.; Jiang, P.; Chen, B.; Zeng, Z. Global Stability of Delayed Genetic Regulatory Networks with Wider Hill Functions: A Mixing Monotone Semiflows Approach. *Neurocomputing* **2023**, *526*, 39−47.
(33) Gonze, D.; Ruoff, P. The Goodwin Oscillator and Its Legacy. *Acta Biotheor.* **2021**, *69*, 857−874.
(34) Gonze, D.; Abou-Jaoude, W. The Goodwin Model: Behind the Hill Function. *PLoS One* **2013**, *8* (8), No. e69573.
(35) Nijland, J. G.; Shin, H. Y.; Dore, E.; Rudinatha, D.; De Waal, P. P.; Driessen, A. J. M. D-Glucose Overflow Metabolism in an Evolutionary Engineered High-Performance D-Xylose Consuming *Saccharomyces cerevisiae* Strain. *FEMS Yeast Res.* **2021**, *21*, No. foaa062.
(36) Brink, D. P.; Borgstrom, C.; Persson, V. C.; Osiro, K. O.; Gorwa-Grauslund, M. F. D-Xylose Sensing in *Saccharomyces cerevisiae*: Insights from D-Glucose Signaling and Native D-Xylose Utilizers. *Int. J. Mol. Sci.* **2021**, *22*, No. 12410.
(37) Colombo, S.; Collini, M.; D'Alfonso, L.; Chirico, G.; Martegani, E. Evidence of Noisy Oscillations of cAMP under Nutritional Stress Condition in Budding Yeast. *Symmetry (Basel).* **2023**, *15*, No. 1793.
(38) Hauser, M. J. B. Synchronisation of Glycolytic Activity in Yeast Cells. *Curr. Genet.* **2022**, *68*, 69−81.
(39) Halder, G.; Dhawane, S. H.; Dutta, D.; Dey, S.; Banerjee, S.; Mukherjee, S.; Mondal, M. Computational Simulation and Statistical Analysis of Bioethanol Production from *Madhuca indica* by Batch Fermentation Process Using *Saccharomyces cerevisiae*. *Sustain. Energy Technol. Assessments* **2016**, *18*, 16−33.
(40) Chalhoub, E. R.; Belovich, J. M. Mathematical Modeling of Fermentation from Glucose, Xylose, and Food Waste of *clostridia sp.* Strain BOH3 for the Production of ABE Solvents and Hydrogen. *Results Eng.* **2024**, *22*, No. 102366.
(41) Beaudeau, F.; Aceves Lara, C. A.; Godilllot, J.; Mouret, J. R.; Trelea, I. C.; Bideaux, C. Modelling the Effects of Assimilable Nitrogen Addition on Fermentation in Oenological Conditions. *Bioprocess Biosyst. Eng.* **2023**, *46*, 941−955.
(42) Luo, H.; Li, P.; Ji, B.; Nielsen, J. Modeling the Metabolic Dynamics at the Genome-Scale by Optimized Yield Analysis. *Metab. Eng.* **2023**, *75*, 119−130.
(43) Klamt, S.; Müller, S.; Regensburger, G.; Zanghellini, J. A Mathematical Framework for Yield (vs. Rate) Optimization in Constraint-Based Modeling and Applications in Metabolic Engineering. *Metab. Eng.* **2018**, *47*, 153−169.
(44) Nosrati-Ghods, N.; Harrison, S. T. L.; Isafiade, A. J.; Tai, S. L. Analysis of Ethanol Production from Xylose Using *Pichia stipitis* in Microaerobic Conditions through Experimental Observations and Kinetic Modelling. *Biochem. Eng. J.* **2020**, *164*, No. 107754.
(45) Naghshbandi, M. P.; Tabatabaei, M.; Aghbashlo, M.; Gupta, V. K.; Sulaiman, A.; Karimi, K.; Moghimi, H.; Maleki, M. Progress toward Improving Ethanol Production through Decreased Glycerol Generation in *Saccharomyces cerevisiae* by Metabolic and Genetic Engineering Approaches. *Renewable Sustainable Energy Rev.* **2019**, *115*, No. 109353.
(46) Heyland, J.; Fu, J.; Blank, L. M. Correlation between TCA Cycle Flux and Glucose Uptake Rate during Respiro-Fermentative Growth of *Saccharomyces cerevisiae*. *Microbiology* **2009**, *155* (12), 3827−3837.
(47) Songdech, P.; Ruchala, J.; Semkiv, M. V.; Jensen, L. T.; Sibirny, A.; Ratanakhanokchai, K.; Soontorngun, N. Overexpression of Transcription Factor ZNF1 of Glycolysis Improves Bioethanol Productivity under High Glucose Concentration and Enhances Acetic Acid Tolerance of *Saccharomyces cerevisiae*. *Biotechnol. J.* **2020**, *15*, No. 1900492.
(48) Conrad, M.; Schothorst, J.; Kankipati, H. N.; Van Zeebroeck, G.; Rubio-Texeira, M.; Thevelein, J. M. Nutrient Sensing and Signaling in the Yeast *Saccharomyces cerevisiae*. *FEMS Microbiol. Rev.* **2014**, *38*, 254−299.
(49) Kim, J. H.; Rodriguez, R. Glucose Regulation of the Paralogous Glucose Sensing Receptors Rgt2 and Snf3 of the Yeast *Saccharomyces cerevisiae*. *Biochim. Biophys. Acta - Gen. Subj.* **2021**, *1865*, No. 129881.
(50) Kim, D.; Song, J. Y.; Hahn, J. S. Improvement of Glucose Uptake Rate and Production of Target Chemicals by Overexpressing Hexose Transporters and Transcriptional Activator Gcr1 in *Saccharomyces cerevisiae*. *Appl. Environ. Microbiol.* **2015**, *81*, 8392−8401.
(51) Busti, S.; Coccetti, P.; Alberghina, L.; Vanoni, M. Glucose Signaling-Mediated Coordination of Cell Growth and Cell Cycle in *Saccharomyces cerevisiae*. *Sensors* **2010**, *10*, 6195−6240.
(52) Peng, B.; Bandari, N. C.; Lu, Z.; Howard, C. B.; Scott, C.; Trau, M.; Dumsday, G.; Vickers, C. E. Engineering Eukaryote-like Regulatory Circuits to Expand Artificial Control Mechanisms for Metabolic Engineering in *Saccharomyces cerevisiae*. *Commun. Biol.* **2022**, *5*, No. 135.
(53) Peng, B.; Plan, M. R.; Carpenter, A.; Nielsen, L. K.; Vickers, C. E. Coupling Gene Regulatory Patterns to Bioprocess Conditions to Optimize Synthetic Metabolic Modules for Improved Sesquiterpene Production in Yeast. *Biotechnol. Biofuels* **2017**, *10*, No. 43.
(54) Van Ende, M.; Wijnants, S.; Van Dijck, P. Sugar Sensing and Signaling in *Candida albicans* and *Candida glabrata*. *Front. Microbiol.* **2019**, *10*, No. 99.
(55) van Rossum, H. M.; Kozak, B. U.; Niemeijer, M. S.; Duine, H. J.; Luttik, M. A. H.; Boer, V. M.; Kotter, P.; Daran, J. M. G.; van Maris, A. J. A.; Pronk, J. T. Alternative Reactions at the Interface of Glycolysis and Citric Acid Cycle in *Saccharomyces cerevisiae*. *FEMS Yeast Res.* **2016**, *16* (3), No. fow017.
(56) Contreras-Ruiz, A.; Alonso-del-Real, J.; Torrat-Noves, J. C.; Barrio, E.; Querol, A. Transcriptional Response of *Saccharomyces cerevisiae* during Competition with *S. kudriavzevii* : Genetic Expression Variability and Accelerated Activation. *Int. J. Food Microbiol.* **2025**, *430*, No. 111053.
(57) Zhou, J.; Arugula, M. A.; Halamek, J.; Pita, M.; Katz, E. Enzyme-Based NAND and NOR Logic Gates with Modular Design. *J. Phys. Chem. B* **2009**, *113*, 16065−16070.
(58) Alipourfard, I.; Datukishvili, N.; Bakhtiyari, S.; Haghani, K.; Di Renzo, L.; de Miranda, R. C.; Mikeladze, D. MIG1 Glucose

https://doi.org/10.1021/acs.iecr.5c01640
Ind. Eng. Chem. Res. XXXX, XXX, XXX−XXX

Repression in Metabolic Processes of *Saccharomyces cerevisiae*: Genetics to Metabolic Engineering. *Avicenna J. Med. Biotechnol.* **2019**, *11* (3), 215−220.
(59) Lu, Z.; Shen, Q.; Liu, L.; Talbo, G.; Speight, R.; Trau, M.; et al. Profiling Proteomic Responses to Hexokinase-II Depletion in Terpene-Producing *Saccharomyces cerevisiae*. *Eng. Microbiol.* **2023**, *3*, No. 100079.
(60) Schrøder, T. D.; Ozalp, V. C.; Lunding, A.; Jernshoj, K. D.; Olsen, L. F. An Experimental Study of the Regulation of Glycolytic Oscillations in Yeast. *FEBS J.* **2013**, *280*, 6033−6044.
(61) Williamson, T.; Adiamah, D.; Schwartz, J. M.; Stateva, L. Exploring the Genetic Control of Glycolytic Oscillations in *Saccharomyces cerevisiae*. *BMC Syst. Biol.* **2012**, *6*, No. 108.
(62) Xiong, L.; Zeng, Y.; Tang, R. Q.; Alper, H. S.; Bai, F. W.; Zhao, X. Q. Condition-Specific Promoter Activities in *Saccharomyces cerevisiae*. *Microb. Cell Fact.* **2018**, *17*, No. 58.
(63) Wang, D.; Wang, L.; Hou, L.; Deng, X.; Gao, Q.; Gao, N. Metabolic Engineering of *Saccharomyces cerevisiae* for Accumulating Pyruvic Acid. *Ann. Microbiol.* **2015**, *65*, 2323−2331.
(64) Patel, M. S.; Nemeria, N. S.; Furey, W.; Jordan, F. The Pyruvate Dehydrogenase Complexes: Structure-Based Function and Regulation. *J. Biol. Chem.* **2014**, *289* (24), 16615−16623.
(65) Solis-Escalante, D.; Kuijpers, N. G. A.; Barrajon-Simancas, N.; van den Broek, M.; Pronk, J. T.; Daran, J. M.; Daran-Lapujade, P. A Minimal Set of Glycolytic Genes Reveals Strong Redundancies in *Saccharomyces cerevisiae* Central Metabolism. *Eukaryot. Cell* **2015**, *14*, 804−816.
(66) Xiong, J.; Xu, H.; Wang, Q.; Sun, W. Improved Synthesis of Deoxyadenosine Triphosphate by *Saccharomyces cerevisiae* Using an Efficient ATP Regeneration System: Optimization of Response Surface Analysis. *Molecules* **2023**, *28*, No. 4029.
(67) Raj, S. B.; Ramaswamy, S.; Plapp, B. V. Yeast Alcohol Dehydrogenase Structure and Catalysis. *Biochemistry* **2014**, *53*, 5791−5803.
(68) Najafpour, G.; Younesi, H.; Ku Ismail, K. S. Ethanol Fermentation in an Immobilized Cell Reactor Using *Saccharomyces cerevisiae*. *Bioresour. Technol.* **2004**, *92*, 251−260.
(69) Krishnamoorthy, U.; Karthika, V.; Mathumitha, M. K.; Panchal, H.; Jatti, V. K. S.; Kumar, A. Learned Prediction of Cholesterol and Glucose Using ARIMA and LSTM Models − A Comparison. *Results Control Optim.* **2024**, *14*, No. 100362.
(70) Medl, M.; Rajamanickam, V.; Striedner, G.; Newton, J. Development and Validation of an Artificial Neural-Network-Based Optical Density Soft Sensor for a High-Throughput Fermentation System. *Processes* **2023**, *11*, No. 297.
(71) Beaudeau, F.; Lara, C. A. A.; Bideaux, C. Dynamic Modelling of the Effects of Assimilable Nitrogen Addition on Aroma Synthesis during Wine Fermentation. *Chem. Eng. Trans.* **2023**, *102*, 301−306.
(72) Tsafrakidou, P.; Manthos, G.; Zagklis, D.; Mema, J.; Kornaros, M. Assessment of Substrate Load and Process PH for Bioethanol Production − Development of a Kinetic Model. *Fuel* **2022**, *313*, No. 123007.

https://doi.org/10.1021/acs.iecr.5c01640
Ind. Eng. Chem. Res. XXXX, XXX, XXX−XXX